Computer-Aided Design of Complex Waveguide Filters for Space Communication Systems

J. V. Morro, C. Bachiller, H. Esteban, V. E. Boria
Instituto de Telecomunicaciones y Aplicaciones Multimedia (iTEAM)
Universidad Politécnica de Valencia
Building 8G, access D, Camino de Vera s/n 46022 Valencia (SPAIN)
Corresponding author: hesteban@dcom.upv.es

Abstract

This paper presents a case study of advanced optimization techniques for the automated design of complex waveguide filters for space application, and a detailed study of the multipactor effect in different H-plane waveguide filters: all metallic, loaded with dielectric cylinders and evanescent mode.

Keywords:multipactor, waveguide filters, dielectric cylinders, space communications, computer aided design, optimization, aggressive space mapping, segmentation, hybridization, genetic algorithms

1. Introduction

There are many reasons that lead to develop new topologies of high frequency filters for space applications, i.e: reduction of mass and volume, increase of thermal stability for high power applications, increase of out-of-band rejection, reduction of manufacturing effort, availability of analysis and design tools for synthesizing a desired response and reduction of risk of radiofrequency breakdown (i.e. Multipactor effect [1], [2]).

Rectangular waveguide H-plane filters are one of the most popular technologies for implementing satellite communications filters, and many efforts are being devoted to improve their capabilities. The development of new topologies in this technology has been historically limited by the availability of CAD tools that allow implementing a filter with a required response and several predefined improvements in terms of mass, stability or high power effects (i.e. multipactor). An efficient Computer-Aided Design (CAD) software package requires a fast and accurate analysis tool for the selected topology and a reliable optimization strategy.

The topologies that are analyzed and designed in this work are rectangular waveguide H-plane filters loaded with cylindrical dielectric posts. When introducing these elements in the filter, the mass and volume are reduced, the thermal stability and the out-of-band rejection are increased, and the risk of radiofrequency breakdown decreases. Moreover, if the dielectric posts are circular the manufacturing effort is dramatically reduced compared to square shapes. However, the accurate modeling of the circular dielectric resonators is far more complex than for square ones, since circular and rectangular geometries must be analyzed together. Other drawback to the use of dielectric loading materials in the filters is the increase of loss level due to the dielectric tangent factor.

This paper begins with a case study of advanced optimization techniques for the automated design of complex waveguide filters for space applications. The accurate design of electromagnetic (EM) structures requires a tradeoff between accuracy and computation time. When designing complex structures, the use of a very accurate simulation tool can be unaffordable. The Aggressive Space Mapping (ASM) methodologies address this issue. Aggressive Space mapping [3] can be used to reduce the computational burden by using two different simulation tools of different accuracy and efficiency: an efficient but not very accurate tool (coarse model) in the optimization space (OS), and an accurate but not very efficient tool (fine model) in the validation space (VS). These methodologies move the computational burden to the OS, thus reducing the overall computation time, while the accuracy is still guaranteed by the use of the fine model. Although ASM has proved to be very useful for EM design, there is still much research dedicated to improve the robustness and performance of ASM [4]. As an alternative to those extensions of ASM, we proposed to improve the ASM approach by using a segmentation and hybridization strategy. The speed and robustness of the optimization process can be greatly improved by decomposing the structure as proposed in [5] and [6]. Moreover, the design process can still be improved by using a suitable combination of several optimization algorithms instead of using a single all-purpose technique such as a genetic algorithm. In this paper, the completely automated CAD tool recently proposed in [7], which does not require human intervention, is adapted for the accurate design of several complex waveguide filters: H-plane coupled cavities filters with and

without tuning elements, and novel designs with dielectric resonators.

Then, this work presents the results for the multipactor effect in the different topologies of filters designed, i.e all metallic ones, filters loaded with circular dielectric posts and evanescent mode filters loaded with dielectric posts (see Fig. 1). The study has been made on the basis of a multimodal analysis method [8] that enables the computation of the electromagnetic fields inside the filter and the dielectric posts in a very accurate and efficient way. The results for such electromagnetic fields have been successfully compared to results obtained with a commercial simulator (Ansoft HFSS [9]). Then a comparative study of the multipactor effect that can appear between the two metallic surfaces of each filter has been performed. In order to achieve a fair comparison, the study was made on several filters with the same frequency response. The filters loaded with dielectric posts are smaller than all the metallic ones, and some of them have also a better out-of-band rejection behavior. Considering the multipactor discharge, the study concludes that the dielectric posts concentrate the electric field inside them, thus producing a smaller level of electromagnetic field outside the dielectric posts than for the all-metallic filters. Following the premise that the multipactor discharge can only appear between the metallic surfaces of the filter, the dielectric loaded filters can handle more power without risk of multipactor breakdown.

2. Aggressive Space Mapping Method

The original ASM strategy describes the behavior of a system by means of two spaces models: the optimization space (OS), denoted by X_{os}, and the validation space (VS), denoted by X_{em}. We represent the designable model parameters in these spaces by the vectors X_{os} and X_{em}, respectively. The objective of the ASM procedure is to find the optimum point X_{em} in VS that minimizes the following non-linear function:

$$f(x_{em})=P(x_{em})-x^{*}_{os} \qquad 1.3$$

where X^{*}_{os} is the optimum point in OS and $P(x_{em})$ is the point in OS that satisfies $R_f(x_{em})=R_c(P(x_{em}))$, R_f and R_c being the vectors with the responses of the fine and coarse models. The ASM procedure finishes when $||f(x_{em})||$ is below some threshold

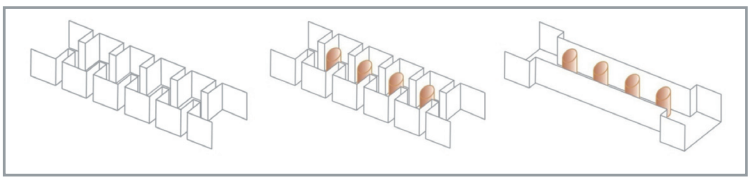

Table 4. Types of filters considered in this work.

η near zero. At each iteration j, the next point is found by a quasi-Newton iteration:

$$x_{em}^{(j+1)} = x_{em}^{(j)} + h^{(j)} \qquad 1.2$$

where $x_{em}^{(0)} = x_{os}^{*}$ and $h^{(j)}$ solves the linear system:

$$B^{(j)} \bullet h^{(j)} = -f^{(j)} \qquad 1.3$$

$B^{(j)}$ is an approximation to the Jacobian matrix and is obtained from $B^{(j-1)}$ using the Broyden update [3].

3. Aggressive Space Mapping with Segmentation and Hybridization

Segmentation

In [4] and [10], a segmentation strategy was proposed for the design of some filter structures, such as H-plane coupled cavity filters composed of N resonant cavities and $N+1$ coupling windows. This segmentation technique transforms a slow multidimensional design process into several efficient and robust design steps, where a small number of parameters are designed at the same time. However, there is the risk that the coupling among all cavities (not just among adjacent cavities) is not properly taken into account. To solve this problem, the segmentation strategy proposed in [11] adds new steps to the original strategy. The resulting new segmentation strategy designs the filter through the steps summarized in Table I.

The Ordinary step designs the parameters related to cavity i simulating the i first cavities, and using for the rest of parameters of the $i-1$ first cavities the values obtained in former iterations. The error function is computed comparing the response of the i first cavities with the ideal response. The ideal response of the i first cavities is obtained using the first i resonators of the prototype composed of impedance inverters and half-

Step	Structure Simulated	Design parameters	Error Function	Performed
Ordinary	i first cavities	Dimensions of cavity i	S_{21}	For each cavity
Coupling	i first cavities	Dimensiones of the first i cavities	S_{21}	Each 3 cavities
Central Cavity	whole	Dimensions of the central cavity	S_{21}	Once
Full Structure	whole	Dimensions of all the cavities	S_{11}	Once

Table 1. *Steps of the proposed segmentation design strategy.*

Both the efficiency and robustness can be drastically improved when a suitable combination of optimization algorithms is used

wavelength transmission lines. The Coupling step adjusts, every three cavities, all the design parameters of the cavities previously designed, thus achieving the required small changes in the values of the parameters due to couplings among cavities. The Central Cavity step designs the dimensions of the central cavity simulating the whole filter structure, and the Final step refines the design taking into account all possible interactions among cavities.

Hybrid Optimization

Both the efficiency and robustness of the optimization process can be drastically improved when a suitable combination of optimization algorithms is used instead of a single algorithm. If only a gradient method is used, it may fail to reach the optimum if the starting point is far from it. On the other hand, the use of a robust method such as the simplex method or genetic algorithm, largely used in circuit design applications, ensures convergence, but at the cost of a low efficiency. So, the design procedure has been improved using a suitable combination of optimization algorithms in each parameter extraction phase and also in the optimization needed to obtain x^*_{os}. Robust non-gradient methods (direct search and simplex) are used at the beginning, and, after some iterations, when we are close to the minimum, an efficient gradient algorithms (Broyden-Fletcher-Goldfarb-Shanno (BFGS)) is used to refine the solution. This combination of algorithms has been proved to perform better than one algorithm alone. The shift from one optimization algorithm to another one is controlled by the parameter termination tolerance xtol, the termination tolerance of the error function (f_{tol}), and the maximum number of function evaluations (nF_{max}) permitted to each method. f_{tol} is higher for the first algorithm, and its value is decreased in each subsequent algorithm. The shift from one algorithm to another, as well as the rest of the whole design process is fully automated, so that no human intervention is needed at all.

4. Multipactor breakdown in waveguide filters

Multipactor effect prediction

The Hatch and Williams [12] model has been used for the study of the multipactor effect inside the filters. In this model, the maximum input power without multipactor breakdown is calculated by using the electric field distribution inside the structure.

In the model, the "Voltage Magnification Factor" VMF [13] is defined as the maximum voltage in the structure versus the input voltage (Vin) for all the frequencies. This factor is calculated for all the points inside the filter and the VMF_{max} is defined as the maximum of $VMFs$. During this work we have found that the maximum of electrical field appeared always in the same point inside the filter, independently of the frequency value. The input threshold power is also a function of the frequency and can be calculated by using the VMFmax, the characteristic impedance Z0 and the threshold voltage Vmulti that enables the multipactor breakdown. This value can be obtained by using Multipactor Calculator [14] and depends on the type of metallic surface and the frequency-gap product.

$$P_{thr}(f) = \frac{1}{VMF^2_{\max}(f)} \frac{V^2_{multi}(f)}{2Z_0} \quad 1.4$$

$$Z_0 = \eta_0 \frac{2b}{a} \frac{\lambda_g}{\lambda} \quad 1.5$$

The minimum of this equation in the whole frequency band provides the maximum power that the device can handle without multipactor breakdown.

Distribution of electromagnetic field inside the filters

This section describes the procedure for obtaining the distribution of electrical field inside the structures as a function of the frequency.

All-metal cavities filter

The field distribution is obtained from the multimodal scattering matrices (GSMs) of each one of the segments that compose the structure of the filter. In Fig. 2 the different segments and matrices are shown. GSMs of the step (S_2, S_4, S_6, S_8...) can be calculated following the well-known Mode Matching Method [15], and the GSMs of the lines (S_1, S_3, S_5, S_7...) are obtained through analytic expressions. The global GSM is obtained using a new efficient recursively connection technique proposed in [16].

Fig. 3 shows the regions where the electric field is calculated. For each region the field distribution is obtained by using the following equation [17]:

$$\vec{E}^i_t(\rho,\phi) = \sum_{m=1}^{M_i} a_m^{(i)} \vec{e}_m^{(i)'} e^{-\gamma_m^{(i)} z_i} + \sum_{m=1}^{M_i} b_m^{(i)} \vec{e}_m^{(i)'} e^{\gamma_m^{(i)} z_i} \quad 1.6$$

where

M_i is the number of modes in the i segment of the filter. Typically M_i=11.

x_i and z_i are the coordinates as defined in Fig. 3.

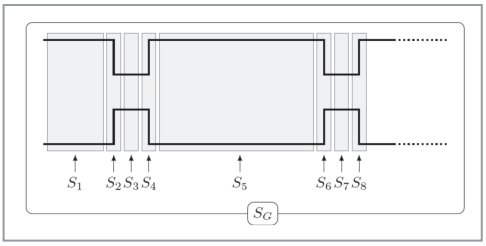

Figure 2. *Segments and GSMs matrices of all-metal cavities filter.*

$a_m^{(i)}$ y $b_m^{(i)}$ are the modal vectors of incident and reflected waves between segments *i-1* and *i* as defined in Fig. 2.

$\vec{e}_m^{(i)'}(x_i)$ is defined in equation.

b_i is the height and a_i the width of each section.

$$\vec{e}_m^{(i)'}(x_i) = \hat{y}_i \sqrt{\frac{2Z_{0m}^{(i)}}{a_i b_i}} \sin\left(\frac{m\pi}{a_i} x_i\right)$$

1.7

Filter loaded with dielectric cylinders

Fig. 4 shows the filter with dielectric cylinders and the different segments in which the filter is divided. There are three different types of segments: lines, steps and segment of line loaded with dielectric cylinder. For each one of them a different method is used for the computation of GSMs and the electric field. As in the previous filter, the GSMs of the steps (S_2, S_4, S_8, S_{10}...) are calculated by using the Mode Matching Method [15] and the GSMs of the lines (S_1, S_3, S_5, S_7...) are computed analytically. For obtaining the GSMs of the segments loaded with dielectric cylinders (S_6,S_{12}...) the hybrid mode matching method is used [17]. Then all the matrices are connected as described in [16] in order to get the global GSM of the filter. For regions *i=1, 3, 5, 6a, 7, 9, 11...* (see Fig. 5) the electric field is calculated as described in the previous subsection. The field in regions *6b, 12b...* (see Fig. 5) is obtained by using the equation , where J_p and $H_p^{(2)}$ are the Bessel and second order Hankel functions, and i_n and c_n are the incident and scattered spectrum coefficients in cylindrical coordinates.

$$\vec{E}^{\text{int}}(\rho,\phi) \approx \sum_{n=-N_i}^{N_i} i_n \cdot J_n(k\rho) \cdot e^{jn\phi} \cdot \hat{z} + \sum_{n=-N_{sc}}^{N_{sc}} c_n \cdot H_n^{(2)}(k\rho) \cdot e^{jn\phi} \cdot \hat{z}$$

1.8

Finally, in regions *6c, 12c...* the field is obtained by the method described in [8], as follows:

$$\vec{E}_t^{\text{int}} = \sum_{n=-N_i}^{N_i} s_n \cdot J_n(k\sqrt{\varepsilon_r \mu_r}\rho) \cdot e^{jn\phi}$$

1.9

where coefficient s_n is:

$$s_n = \frac{\begin{vmatrix} -H_n^{(2)}(kr) & J_n(kr) \\ -H_n^{(2)'}(kr) & J_n'(kr) \end{vmatrix}}{\begin{vmatrix} -H_n^{(2)}(kr) & J_n(k\sqrt{\varepsilon_r\mu_r}r) \\ -H_n^{(2)'}(kr) & \frac{\sqrt{\varepsilon_r}}{\sqrt{\mu_r}} J_n'(k\sqrt{\varepsilon_r\mu_r}r) \end{vmatrix}} i_n$$

1.10

and *r* the radius of the dielectric post.

Evanescent mode filter loaded with dielectric cylinders

In an evanescent mode filter, the fundamental mode TE_{10}, is below the cutoff frequency in the narrow waveguide, while it is propagating in the input wider waveguide.

The procedure followed to calculate the field inside this filter is similar to the methodology described in the two previous sections.

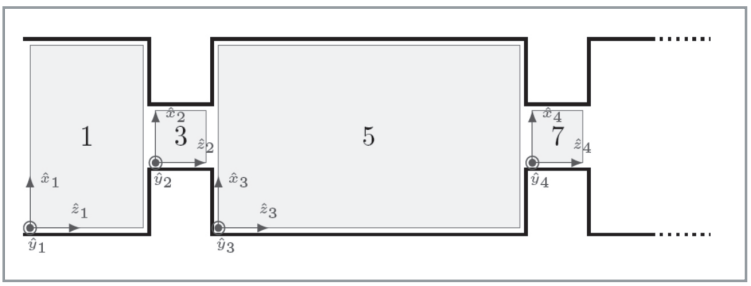

Figure 3. *Regions for the computation of the electric field.*

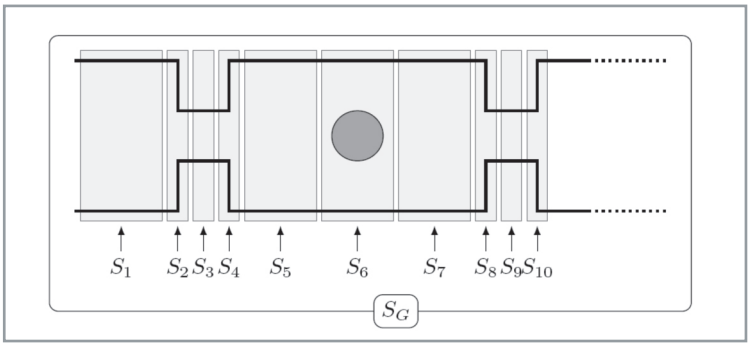

Figure 4. *Segments and GSMs matrices of the filter loaded with dielectric cylinders.*

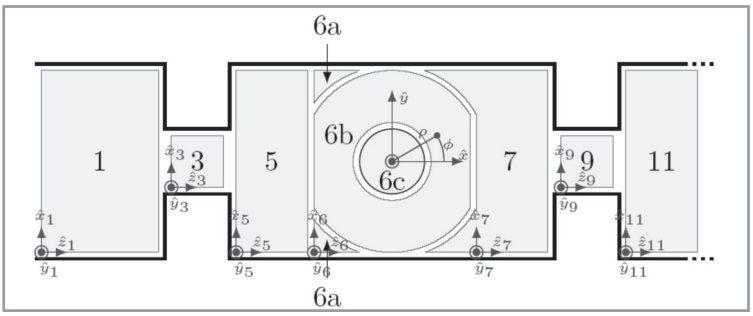

Figure 5. *Regions for the calculation of electric field of the filter loaded with dielectric cylinders.*

5. Results

High-Order H-plane waveguide filter for space applications at K-Band

The first example under consideration is a conventional H-plane waveguide filter with coupled cavities for space applications at the K-band. The ideal transfer function is a standard nine-pole Chebychev response of 96 MHz bandwidth centered at 17.3 GHz.

The cavity lengths and coupling aperture widths of the filter have been chosen as design parameters (see Fig. 8). The input and output waveguides of the filter, as well as the resonant cavities, are standard WR-62 waveguides (a=15.799 mm,

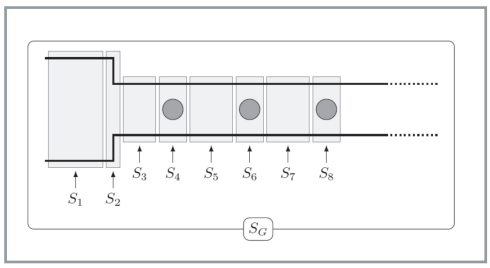

Figure 6. *Segments and GSMs matrices of evanescent filter with dielectric cylinders*

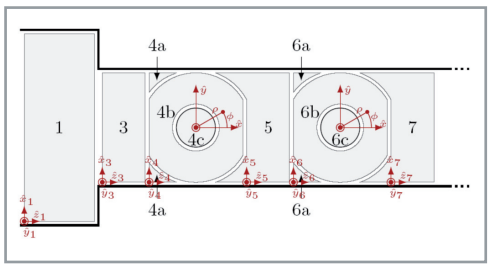

Figure 7. *Regions for calculating the electric field of the evanescent filter with dielectric cylinders.*

b=7.899 mm). The length of all the coupling windows has been chosen to be 2 mm. For the design of this filter, the same modal simulator has been used both as the coarse and the fine model. This modal simulator characterizes the planar discontinuities using the Method of the Moments (MoM) according to the traditional Galerkin procedure [18]. When used as a fine model, the number of accessible modes, number of basis functions in the MoM, and number of kernel terms in the integral-equation are high enough to obtain very accurate results. On the other hand, when used as a coarse model, a small number of modes is considered in order to obtain a faster simulator at the expense of a less accuracy. The initial values of the design parameters $(x_{os}^{(0)})$ have been calculated according to the method described in [19]. Fig. 9 shows the comparison between the response of the fine model at the final solution in VS (x_{em}) and the response of the coarse model at x_{os}^*. It can be observed that the desired objective function has been satisfactorily recovered in the VS. This solution has required 185 s of CPU time in a 2.4 GHz Pentium IV PC platform.

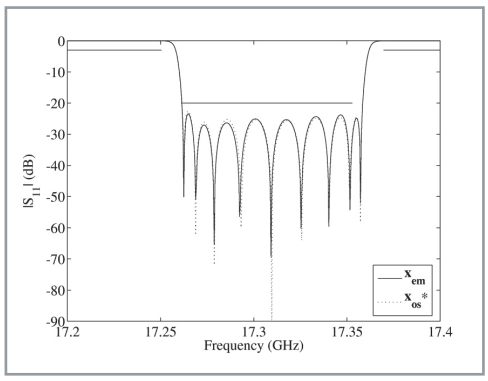

Figure 9. *Responses of the H-plane waveguide filter. Coarse model response at x_{os}^* versus the fine model response at xem.*

Tunable H-plane waveguide filter for space communication systems

In order to test the performance of the design procedure with more complex structures, two tunable H-plane coupled cavity filters have been considered. These filters were originally designed and manufactured in [20], where the design was performed manually. The same filters have been re-designed with the CAD tool proposed in this work. The tuning elements are penetrating posts of square cross-section placed at the center of each cavity and each coupling window (see Fig. 10). As proposed in [20], the use of these tuning posts allows the use of a common base structure for obtaining filters with responses centered at different frequency bands. The only difference in the filters at each frequency band is the penetration of the tuning posts.

The ideal transfer function is a four-pole standard Chebychev band-pass response of 300 MHz bandwidth centered at 11 GHz and 13 GHz. The input and output waveguides of the filter, as well as the resonant cavities, are standard WR-75 waveguides *(a=19.050 mm, b=9.525 mm)*. The length of all the coupling windows has been chosen to be 2 mm. The sides of the posts are fixed to 4 mm in the cavities and 2 mm in the coupling windows.

The design with ASM using segmentation and hybrid optimization required 3 ASM iterations for both filters under severe convergence cri-

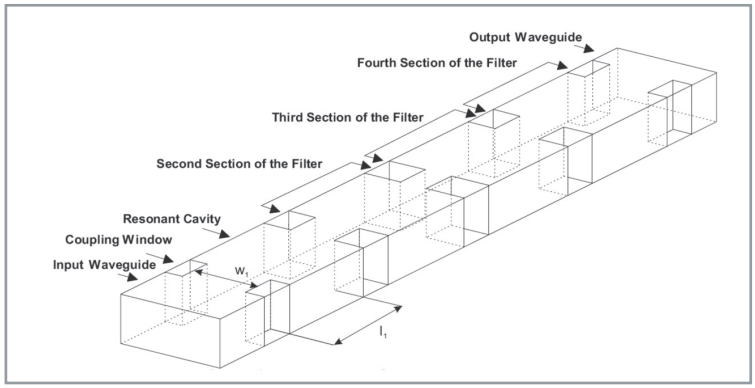

Figure 8. *A four cavities H plane rectangular waveguide filter.*

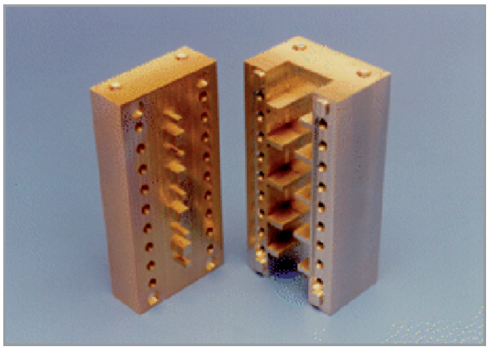

Figure 10. *Manufactured tunable filters with tuning elements. Common base and 11 GHz top.*

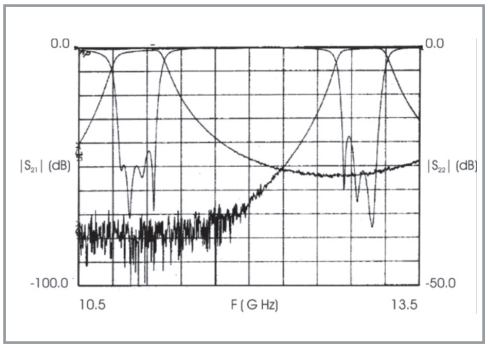

Figure 11. *Measurements of the manufactured prototypes with tuning elements.*

terion. The design for the filters centered at 11 and 13 GHz required a total CPU times of 49'50" and 33'42", respectively, in a PC with Pentium IV processor at 1.7 GHz. Since the fine model is about 250 times slower than the coarse model, the total CPU time required for the direct design of such filters without ASM would be of about 25 hours. This represents an improvement by a factor of 30, and clearly proves the advantage of using ASM for the design of complex waveguide devices. The filters have been manufactured in two different pieces, an H-plane base structure and a separated top cover including all the tuning elements. To reduce costs, the same H-plane base has been used for both filters. The common H-plane base and the two different tops including the tuning elements for the filters at 11 and 13 GHz were manufactured (see Fig. 10) and measured (see Fig. 11).

H-plane waveguide filter with dielectric resonators

The last structure under consideration is an H-plane coupled cavities filter with circular dielectric posts placed in the middle of each cavity (see Fig. 12(a)). The ideal transfer function is a standard four-pole Chebychev response of 300 MHz bandwidth centered at 11 GHz. The input and output waveguides of the filter, as well as the resonant cavities, are standard WR-75 waveguides (a=19.05 mm, b=9.525 mm). The relative permittivity of the dielectric posts is chosen to be 24, and the length of all the coupling windows have been chosen to be 2 mm. The remaining dimensions of the structure (cavity lengths, coupling aperture widths and radii of the dielectric posts) have been chosen as design parameters. The design procedure described in section III can not be directly applied to the design of this kind of filters. It is necessary to use a genetic algorithm, since a good starting point can not be easily obtained, as well as to suppress the segmentation strategy, since the coupling among cavities is much stronger that in all-metallic filters. Again the same simulation tool is used as the coarse and fine model. This simulation tool is described in [21]. It uses a suitable combination of an analytical method and a hybrid technique which copes with the different parts of the filter structure. Fig. 12(b) shows the comparison between the response of the fine model at xem and the ideal response of the filter. It can

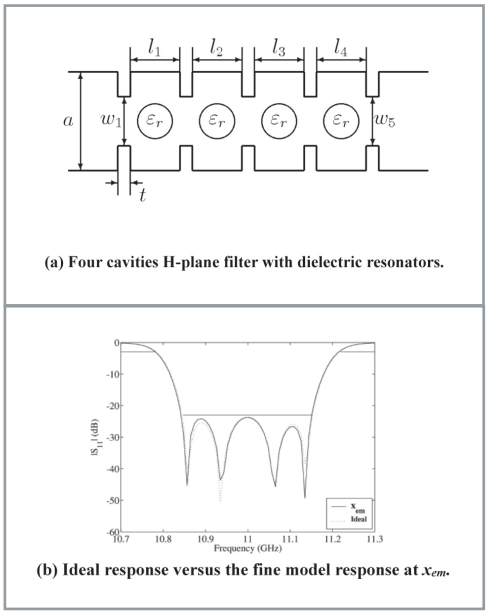

Figure 12. *H-plane waveguide filter with dielectric resonators.*

be observed that the desired objective function has been satisfactorily recovered in the VS. This solution has required about 2 hours of CPU time in a 3 GHz Pentium IV platform. The total length of the filter *(l1+l2+l3+l4+5t)* is reduced by almost 50% when compared with the same filter without dielectric posts, with the correspondent benefit in terms of volume and mass reduction, so critic in satellite communication systems.

Comparative study of multipactor breakdown

The last part of this work evaluates the risk of multipactor breakdown in a set of filters. In order to have a fair comparison the filters should provide the same frequency response, so we designed three different filters: all metal cavities, cavities loaded with dielectric cylinders and evanescent mode loaded with dielectric cylinders filters, which present the same frequency response shown in Fig. 13.

It is important to notice that during the work we have considered that the multipactor breakdown can only appear between two electric plates containing a normal field, so for the calculation of the power that a particular filter can handle we have used the field inside that filter but outside the dielectric cylinders. All the dielectric cylinders used in the filters have a dielectric permittivity $\mathcal{E}r=24$.

All-metal cavities filter

During the study the authors found that the maximum of the electric field was always located on the central longitudinal axis of the filter, and in the middle of the second cavity independently of the frequency value. Fig. 14 shows the maximum input and output power without multipactor breakdown as a function of the frequency. It is interesting that inside the pass band the amount of input and output power that the filter can handle is the same, around 2500 W, and that

A different method is used for the analysis of each type of building block

A higher losses dielectric reduces the power handling capability

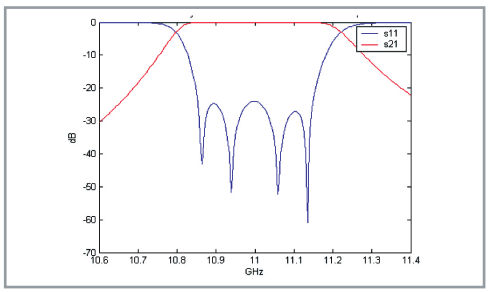

Figure 13. *Scattering parameters S11 and S21 of the H-plane filters under study.*

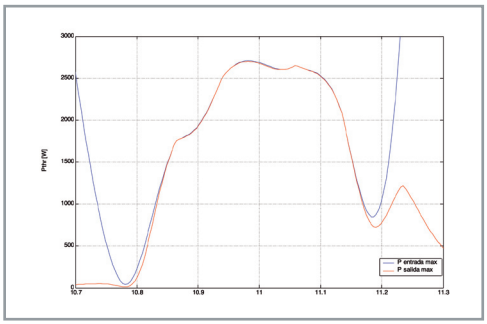

Figure 14. *Maximum input and output power that the all-metal cavities filter can handle without multipactor breakdown as a function of frequency.*

outside this band the power is not limited by the multipactor risk but by the electromagnetic response of the filter.

Filter loaded with dielectric cylinders

In this filter the electric field was concentrated inside the dielectric cylinders, specifically there was a maximum of field inside the second cylinder, being the maximum of field outside the dielectric cylinders considerably lower than in the case of the all-metal filter. Nevertheless, loading the filters with a dielectric material can introduce losses in the filter response that can affect the output power that the filter can handle. Fig. 15 shows the output power that the filter can handle without the risk of multipactor breakdown for dielectric materials with different loss factors. Even with a loss tangent of 10^{-3} this filter can handle the double of power than the all-metal one. Moreover, with a rather high quality factor *($tg\delta=10^{-4}$)* the behavior of the filter does not divert from the ideal (lossless) case.

Evanescent mode filter loaded with dielectric cylinders

The evanescent mode filter is substantially smaller than the all-metal one, which makes that the electric field is more concentrated in the filter and that the risk of multipactor breakdown increases. Nevertheless, when loading this filter with dielectric cylinders, the output power without multipactor breakdown (see Fig. 16) can be higher than in the all-metal filter, since the field trends to concentrate inside the dielectric cylinders. The figure also shows the output power for different dielectric materials, with different loss tangent factors, concluding that a good quality factor dielectric *($tg\delta=10^{-4}$)* can provide a power response similar to the ideal one, while a worse dielectric reduces this power handling but maintains it above the all-metal one.

	Filter 1: all-metal	Filter 2: cavities with dielectric	Filter 3: evanescent with dielectric
Total lenght	96.57mm	60.52mm	56.19mm

Table 2. *Lenghts of the three filters.*

	Filter 1	Filter 2	*Filter 3*
E max (inside dielectric)	-	11357 V/m	*17166 V/m*
Frequency	-	11.188 GHz	*11.24 GHz*
E max (outside dielectric)	14618 V/m	9987 V/m	*14281 V/m*
Frequency	*10.816 GHz*	*10.82 GHz*	*10.772 GHz*

Table 3. *Maximum field ($tg\delta$ =1e-4)*

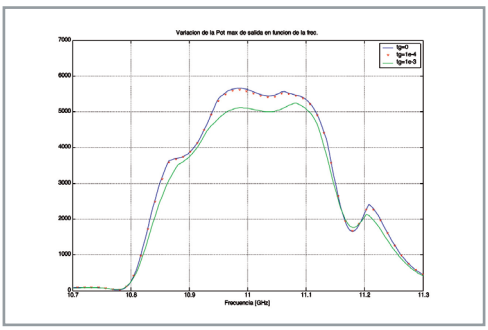

Figure 15. *Maximum output power without multipactor breakdown for the cavities filter loaded with dielectric cylinders, loss tangents $tg\delta=0$, $tg\delta=10^{-3}$, $tg\delta=10^{-4}$*

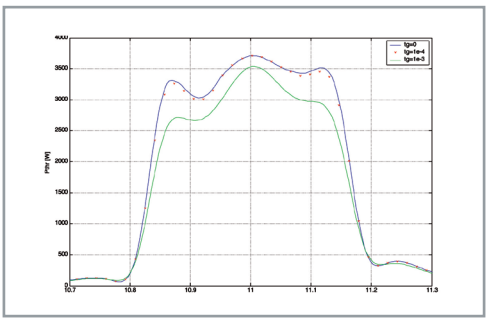

Figure 16. *Maximum output power without multipactor breakdown for the evanescent mode filter loaded with dielectric cylinders, loss tangents $tg\delta=0$, $tg\delta=10^{-3}$, $tg\delta=10^{-4}$*

Comparison of results

It is interesting to show a comparative study of the three filters considering three relevant items: size, maximum field inside the filters and maximum output power without multipactor risk. Table II lists the total length of the three filters. The evanescent filter presents a reduction in size of about 50% comparing to the all-metal case, and the cavities filter with dielectric cylinders is about 60% of the original size. The following table presents the maximum value of the electric field inside the filters, for both cases: inside the dielectric cylinders and outside them. When having filters loaded with dielectric materials, the maximum of field is always located inside the dielectric cylinders. This phenomenon enables the increase of power without risk of multipactor as shown in Fig. 17. Fig. 17 presents

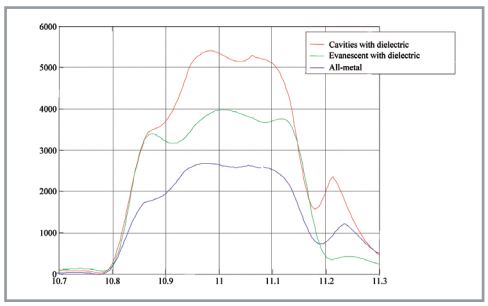

Figure 17. *Comparative chart of the output power for all the filters (dielectric loss factor: tgδ =1e-4).*

a comparative of the maximum output power without multipactor risk for the three filters under analysis considering that the filters loaded with dielectric cylinders present low losses *($tg\delta=10^{-4}$)*. It can be observed that the cavity filter loaded with dielectric cylinders can handle more than double the power of an all-metal filter.

Conclusions

A case study of advanced optimization techniques for the automated design of complex waveguide filters for space applications has been presented in this paper. A complete automated design tool has been developed based on ASM enhanced with segmentation and hybridization schemes. This tool has been successfully applied to the practical design of H-plane coupled cavities filters with and without tuning elements, and for the design of H-plane filters with dielectric posts. The multipactor effect in the filters designed with our CAD tool has been analyzed following a novel analysis technique that enables also the computation of the electromagnetic field inside the structure.

Acknowledgment

The authors would like to thank Dr. M. Guglielmi, European Space Research and Technology Center (ESTEC)-European Space Agency (ESA), Noordwijk, The Netherlands, for providing prototypes and measurements of real filters considered in this paper.

References

[1] R. Udiljak, "Multipactor in Low Pressure Gas". Master Thesis. Department of Electromagnetics, School of Electrical Engineering, Chalmers University of Technology, Göteborg, Sweden 2004.

[2] R. Udiljak, "Multipactor in Low Pressure Gas and in Nonuniform RF Field Structures". PhD Thesis Department of Radio and Space Science, Chalmers University of Technology, Göteborg, Sweden 2007.

[3] J. Bandler, R. Biernacki, S. Chen, R. Hemmers, and K. Madsen, "Electromagnetic optimization exploiting aggressive space mapping," IEEE Trans. Microwave Theory Tech., vol. 43, no. 12, pp. 2874-2881, Dec. 1995.

[4] J. W. Bandler, S. Cheng, Q. S.and Dakroury, A. S. Mohamed, K. Bakr, M. H. Madsen, and J. Söndergaard, "Space mapping: The state of the art," IEEE Trans. Microwave Theory Tech., vol. 52, no. 1, pp. 337-361, Jan. 2004.

[5] M. Guglielmi, "Simple CAD procedure for microwave filters and multiplexers," IEEE Trans. Microwave Theory Tech., vol. 42, no. 7, pp. 1347-1352, July 1994.

[6] J. T. Alos and M. Guglielmi, "Simple and effective EM-based optimization procedure for microwave filters," IEEE Trans. Microwave Theory Tech., vol. 45, no. 5, pp. 856-858, May 1997.

[7] J. V. Morro, P. Soto, H. Esteban, V. Boria, C. Bachiller, M. Taroncher, S. Cogollos, and B. Gimeno, "Fast automated design of waveguide filters using aggressive space mapping with a new segmentation strategy and a hybrid optimization algorithm," IEEE Trans. Microwave Thoery Tech., vol. 53, no. 4, pp. 1130-1142, April 2005.

[8] H. Esteban, S. Cogollos, V. E. Boria, A. A. San Blas, M. Ferrando "A New Hybrid Mode-Matching/ Numerical Method for the Analysis of Arbitrarily Shaped Inductive Obstacles and Discontinuities in Rectangular Waveguides". IEEE Trans. Microwave Theory Tech., vol. 50, no. 4, pp. 1219–1224, April, 2002.

[9] Ansoft Corporation. [Online] http://www.ansoft.com/products/hf/hfss/. HFSS: 3D Electromagnetic Simulation. 2008.

[10] M. Guglielmi, "Simple CAD procedure for microwave filters and multiplexers," IEEE Trans. Microwave Theory Tech., vol. 42, no. 7, pp. 1347-1352, July 1994.

[11] J. V. Morro, H. Esteban, P. Soto, V. E. Boria, C. Bachiller, S. Cogollos, and B. Gimeno, "Automated design of waveguide filters using aggressive space mapping with a segmentation strategy and hybrid optimization techniques," in Proc. of the IEEE Int. Microwave Symp., Philadelphia, June 2003, pp. 1215-1218.

[12] A.J.Hatch, H.B.Williams, "The secondary electron resonance mechanism of low-pressure high-frequency gas breakdown". Journal of Applied Physics, vol. 25, pp. 417-423. April 1954.

[13] A. V. M. Ludovico, G. Vercellino and L. Accatino, "Multipaction análisis in high power antenna diplexers for satellite applications" Proceedings of the Workshop on Multipactor, RF and DC Corona and Passive Intermodulation in Space RF Hardware, pp. 109. ESTEC, Noordwijk, The Netherlands September, 2000.

[14] ESA/ESTEC. Multipactor Calculator. [Online] http://multipactor.esa.int/index.html. April 2007

[15] J.M.Reiter, F.Arndt "Rigorous analysis of arbitrarily shaped H- and E-plane discontinuities in rectangular waveguides by a full-wave boundare contour mode-matching method". IEEE Trans. on Microwave Theory and Tech, vol. 43, no. 4, pp. 796-801. April 1995.

[16] C.Bachiller, H.Esteban, V.E.Boria, A.Belenguer, J.V.Morro. "Efficient Technique for the Cascade Connection of Multiple Two Port Scattering Matrices". IEEE Transactions on Microwave

Theory and Techniques, vol. 55, no. 9, pp 1880-1886, September 2007
[17] H. Esteban, "Análisis de Problemas Arbitrarios de Dispersión Electromagnética Mediante Métodos Híbridos", PhD Thesis, Departamento de Comunicaciones, Universidad Politécnica de Valencia, Spain 2002.
[18] G. Gerini, M. Guglielmi, and G. Lastoria, "Efficient integral equation formulations for admittance or impedance representation of planar waveguide junctions," IEEE MTT-Symp. Dig., vol. III, pp. 1747-1750, 1998.
[19] P. Soto, J. Gómez, A. Bergner, V. E. Boria, and R. Chismol, "Automated design of waveguide filters using space mapping optimization," in Proc. of 3rd Eu. Conf. on Numerical Meth. in Electromagnetism, Poitiers, March 2000, pp. 228-229.
[20] V. E. Boria, M. Guglielmi, and P. Arcioni, "Computer-aided design of inductively coupled rectangular waveguide filters including tuning elements," Int. J. of RF and Microwaves Computer-Aided Engineering, vol. 8, no. 3, pp. 226-236, May 1998.
[21] C. Bachiller, H. Esteban, V. E. Boria, J. Morro, L. Rogla, M. Taroncher, and A. Belenguer, "Efficient CAD tool fo direct-coupled-cavities filters with dielectric resonators," in 2005 IEEE AP-S Int. Symp. Dig., Washington D.C., June 2005.

Biographies

José Vicente Morro received the Telecommunications Engineering degree from the Universidad Politécnica de Valencia (UPV), Valencia, Spain, in 2001, and is currently pursuing his Ph.D. degree at UPV. In 2001, he became a Research Fellow with the Departamento de Comunicaciones, UPV. In 2003 he joined the Signal Theory and Communications Division, Universidad Miguel Hernández, where he was a Lecturer. In 2005, he rejoined the Departamento de Comunicaciones, UPV, as an Lecturer. His current interests include CAD design of microwave devices and EM optimization methods.

Carmen Bachiller received her degree in Communication Engineering from the Polytechnic University of Valencia in 1996. She worked from 1997 to 2001 in the company ETRA I+D, S.A as a Project Engineer in research and development on automatic traffic control, public transport management and public information systems using telecommunication technology. In 2001 she joined the Communication Department of the Polytechnic University of Valencia as an assistant lecturer. She is secretary of the iTEAM Institute of Multimedia Technology and Communications of the Polytechnic University of Valencia. She is teaching signal and systems theory and microwaves. She has participated in several teaching innovation projects as the development of GUIs for teaching electromagnetic phenomena. She is now working in her Ph.D. Thesis on electromagnetism and radiofrequency circuits.

Héctor Esteban González received the degree in Telecommunications Engineering from the Polytechnic University of Valencia (UPV), Spain, in 1996, and the Ph.D. degree in 2002. He collaborated with the Joint Research Centre, European Commission, Ispra, Italy. In 1997, he was with the European Topic Centre on Soil (European Environment Agency). He rejoined the UPV in 1998. His research interests include methods for the full- wave analysis of open-space and guided multiple scattering problems, CAD design of microwave devices, electromagnetic characterization of dielectric and magnetic bodies, and the acceleration of electromagnetic analysis methods using the wavelets and the FMM.

Vicente E. Boria Esbert received the Ingeniero de Telecomunicación and the Doctor Ingeniero de Telecomunicación degrees from the Universidad Politécnica de Valencia, Valencia, Spain, in 1993 and 1997, respectively. In 1993 he joined the Departamento de Comunicaciones, Universidad Politécnica de Valencia, where he is Full Professor (since 2003). In 1995 and 1996 he was held a Spanish Trainee position with the European Space research and Technology Centre (ESTEC)-European Space Agency (ESA), Noordwijk, the Netherlands. Since 2003, he has served on the Editorial Boards of the IEEE Transactions on Microwave Theory and Techniques. He is also member of the Technical Committees of the IEEE-MTT International Microwave Symposium and of the European Microwave Conference. His current research interests include numerical methods for the analysis of waveguide and scattering structures, automated design of waveguide components, radiating systems, measurement techniques, and power effects in passive waveguide systems.